

Quantitative Efficiency and Temperature Analysis of Battery-Ultracapacitor Hybrid Energy Storage Systems

Chen Zhao, *Student Member, IEEE*, He Yin, *Student Member, IEEE*, Chengbin Ma, *Member, IEEE*

Abstract—This paper provides quantitative analysis on system efficiency and battery temperature rise in battery-alone system, passive, battery semiactive, capacitor semiactive hybrid energy storage systems (HESSs). First the system efficiencies and the temperature rises in battery are derived under a pulsed load profile and the four different topologies. Sensitivity analysis is then performed to investigate the influences of the factors (the characteristics of the load profile, the state of charge of battery, and the efficiency of the dc-dc converter) on the four energy storage systems. The proper usage of the HESSs is discussed later based on the results of the sensitivity analysis. It is found that in the most cases the capacitor semiactive HESS is superior in both system efficiency and the suppression of the battery temperature rise. Meanwhile, its behavior is more complicated than that of the battery semiactive HESS. The battery semiactive HESS is suitable for the highly dynamic loads, but its performance more depends on the efficiency of the dc-dc converter. Finally experiments are conducted that validate the previous theoretical discussions.

Index Terms—Battery, ultracapacitor (UC), hybrid energy storage system (HESS), efficiency, temperature, quantitative analysis.

I. INTRODUCTION

The efficient utilization of renewable energy resources (e.g., solar and wind energy, etc.) is a crucial solution for minimizing emission of greenhouse gases [1]. Due to the intermittent nature of the sources, energy storage systems are usually needed to compensate and prevent load fluctuations [2]. So far, batteries are the most popular energy storage devices to meet the requirements of emerging applications in sustainable energy systems such as electric vehicles and microgrids. However, dynamically changing load demand causes oversized battery packs, shortened battery cycle life, and lowered energy efficiency [3]. A possible solution is to use ultracapacitors (UCs), an assistive energy storage device, that meet the dynamic load demand and improve the efficiency, reliability (e.g., protection of battery), and dynamic response of the

overall system [4]. UCs provide fast and efficient energy delivery thanks to their high power density, two to three times higher than that of the most batteries [5]. However, at present the energy density of UCs is very low, less than one tenth of that of the lithium-ion batteries [5]. Combination of batteries and UCs is considered to be the best usage of UCs in real applications that meets the load requirement and takes the advantage of the complementary features of the two devices [6]. Various battery-UC hybrid energy storage systems (HESSs) were developed in recent years for the transportation and utility applications [7].

Generally there are three types of topologies for battery-UC HESSs, passive, semiactive, and fully active topologies [8]. The passive HESS is the simplest topology, in which batteries and UCs are directly connected in parallel. Compared to the battery-alone system, the passive HESS shows an obvious improvement on peak power capability under a pulsed load profile [9]. However, the passive HESS cannot fully utilize the UCs due to the uncontrollable current flow. By adding dc-dc converters, the current flow can be properly distributed to improve the system performances of both semiactive and fully active HESSs. These active HESSs can be actively controlled to let UCs supply the most of the dynamic load, and thus further improve the peak power capability [10]. This advantage leads to a reduced peak current and an extended cycle life of the batteries [11], [12]. Meanwhile, the energy loss from the dc-dc converter itself degrades the system efficiency [13]. Taking into account of the loss in the dc-dc converter, the semiactive HESS is optimally controlled and experimentally demonstrates a higher efficiency than the battery-alone system [14], [15]. However, these existing results are all discussed under specific load profiles in target applications. As to the knowledge of the authors, there is a lack of a quantitative study on the performances of the battery-UC HESSs under various topologies and operating conditions.

As discussed above, the main objectives of adopting the battery-UC HESSs are to improve the system efficiency, battery cycle life, and the dynamic response of the energy storage systems. It is straightforward to understand the improvement in the dynamic response because of the large difference between the power densities of batteries and UCs. However, for the influences on the system efficiency and the extension of the battery cycle life, a comprehensive study is needed to quantitatively analyze and compare the different topologies under a dynamic load profile. This effort is important to further understand the natures of the HESSs and guide real

© 2016 IEEE. Personal use of this material is permitted. Permission from IEEE must be obtained for all other uses, including reprinting/republishing this material for advertising or promotional purposes, collecting new collected works for resale or redistribution to servers or lists, or reuse of any copyrighted component of this work in other works.

Manuscript received December 15, 2015; revised May 5, 2016; accepted May 20, 2016. This work was supported by the National Science Foundation of China under Grant 50950110341 (2010) and Grant 51375299 (2014–2017), and in part by Nippon Chemi-con Corporation.

C. Zhao, H. Yin, and C. Ma are with the University of Michigan-Shanghai Jiao Tong University Joint Institute, Shanghai Jiao Tong University, Shanghai 200240, China (e-mail: zc437041363@sjtu.edu.cn; yyy@sjtu.edu.cn; chbma@sjtu.edu.cn). C. Ma is also with the School of Mechanical Engineering, Shanghai Jiao Tong University, Shanghai 200240, China.

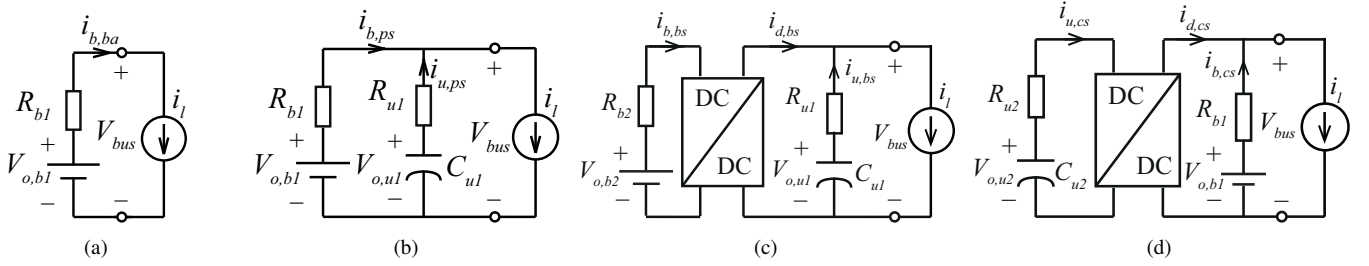


Fig. 1. Equivalent circuit models. (a) Battery-alone system. (b) Passive HESS. (c) Battery semiactive HESS. (d) Capacitor semiactive HESS.

applications. In the following sections, the system efficiencies and the temperature rises in battery are first derived for the conventional battery-alone system, and the three most common battery-UC HESSs, the passive, battery and capacitor semiactive HESSs, under a pulsed load profile [see Fig. 1]. Compared with the fully active HESS, the semiactive HESSs are considered to be a practical solution in terms of reduced complexity and losses because only a single dc-dc converter is required [8]. The temperature rise in battery is chosen because it is a key factor that affects the battery cycle life [16]. The Sobol' indice-based sensitivity analysis is then performed to determine the most influential factors for the system efficiency and the battery temperature rise in the different HESS topologies. This enables quantitative discussions on the proper usage of the HESSs that best fits the requirements from a target application. Finally experiments are conducted for validation purposes.

II. DERIVATIONS OF EFFICIENCY AND TEMPERATURE

In order to facilitate the following quantitative analysis, a pulsed current load is used to represent a dynamic load profile [17]. As shown in Fig. 2, the pulsed load current i_l can be decomposed into two components, a constant average current $I_{l,a}$ and a dynamic current with magnitudes of $I_{l,dp}$ and $I_{l,dn}$, namely

$$i_l = \begin{cases} I_{l,min} = I_{l,a} - I_{l,dn} & \text{if } 0 < t \leq (1-D)T, \\ I_{l,max} = I_{l,a} + I_{l,dp} & \text{else,} \end{cases} \quad (1)$$

and

$$I_{l,a} = (1-D)I_{l,min} + DI_{l,max}, \quad (2)$$

where T and D are the single period and the duty cycle of the pulsed current load, respectively; $I_{l,max}$ and $I_{l,min}$ are the maximum and minimum load currents, respectively. Substituting (1) into (2) gives the relationships among $I_{l,dn}$, $I_{l,dp}$, and D ,

$$I_{l,dn} = D(I_{l,dp} + I_{l,dn}) \text{ and } I_{l,dp} = (1-D)(I_{l,dp} + I_{l,dn}). \quad (3)$$

A state-space approach usually can give compact representations [18]. Due to the nonlinearities of the load profile and the models discussed below, differential equations are directly used to represent the current-voltage relationships in the four energy storage systems.

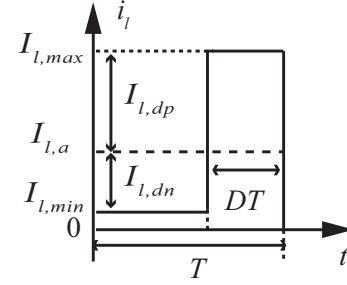


Fig. 2. The pulsed current load during a single period T .

A. Battery-alone System

In this system the battery pack is directly connected to the load, as shown by its equivalent circuit model, Fig. 1(a). Here the internal resistance, R_{b1} , and open circuit voltage (OCV), $V_{o,b1}$, are obtained using a fast averaging method, and represented by two six-ordered polynomials of battery state-of-charge (SOC) through curve fitting [19].

$$V_{o,b1} = a_0 + a_1x + a_2x^2 + \dots + a_6x^6, \quad (4)$$

$$R_{b1} = b_0 + b_1x + b_2x^2 + \dots + b_6x^6, \quad (5)$$

where x is a specific SOC of the battery pack; a_i and b_i ($i = 0, \dots, 6$) are the fitted coefficients, as listed in Table I. Assuming the OCV of the battery is constant over the period T , the system efficiency η_{ba} can be calculated as

$$\eta_{ba} = \frac{\int_0^T V_{o,b1} i_l dt - \int_0^T i_l^2 R_{b1} dt}{\int_0^T V_{o,b1} i_l dt}. \quad (6)$$

From the definitions of i_l and $I_{l,a}$, (1) and (2), η_{ba} can be rewritten as

$$\begin{aligned} \eta_{ba} &= 1 - \frac{I_{l,min}^2(1-D)R_{b1} + I_{l,max}^2DR_{b1}}{V_{o,b1}I_{l,a}}, \\ &= 1 - \frac{(I_{l,a} - I_{l,dn})^2(1-D)R_{b1} + (I_{l,a} + I_{l,dp})^2DR_{b1}}{V_{o,b1}I_{l,a}}. \end{aligned} \quad (7)$$

From the relationships in (3), it can be further written as

$$\begin{aligned} \eta_{ba} &= 1 - \frac{I_{l,a}^2R_{b1} + (1-D)D(I_{l,dp} + I_{l,dn})^2R_{b1}}{V_{o,b1}I_{l,a}}, \\ &= 1 - \frac{I_{l,a}^2R_{b1} + I_{l,dp}I_{l,dn}R_{b1}}{V_{o,b1}I_{l,a}}. \end{aligned} \quad (8)$$

TABLE I
PARAMETERS OF BATTERY AND UC PACKS.

Battery Pack (4S2P)													
a_0	12.38	a_1	29.02	a_2	-129.51	a_3	299.09	a_4	-366.81	a_5	231.77	a_6	-59.23
b_0	0.49	b_1	-4.72	b_2	28.51	b_3	-83.27	b_4	125.62	b_5	-94.10	b_6	27.67
Battery Pack (2S4P)													
a_0	6.38	a_1	11.99	a_2	-51.75	a_3	116.28	a_4	-138.41	a_5	85.11	a_6	-21.23
b_0	0.13	b_1	-1.29	b_2	7.77	b_3	-22.50	b_4	33.64	b_5	-25.02	b_6	7.32
UC Pack (8S1P)				UC Pack (4S2P)				Battery thermal model					
C_{u1}	40F	R_{u1}	60 m Ω	C_{u2}	160F	R_{u2}	20 m Ω	h	0.051 WK ⁻¹	C_p	60.62 JK ⁻¹		

TABLE II
ENTROPIC HEAT COEFFICIENT VERSUS BATTERY SOC.

SOC _b	0.1	0.2	0.3	0.4	0.5	0.6	0.7	0.8	0.9
$\frac{\partial V_{ocv}}{\partial T_b}$ [mVK ⁻¹]	-1.82	-0.68	-0.53	-0.26	-0.19	-0.18	-0.11	-0.17	-0.18

As discussed in the introduction, the battery cycle life is strongly affected its temperature [16]. It is intuitive that with the UCs to provide the dynamic current, the temperature rise in the batteries could be reduced, namely extended battery cycle life. However, this important aspect should also be quantitatively discussed and analyzed. In this paper the below battery thermal model is used for analysis purposes,

$$C_p \frac{dT_b}{dt} = -h(T_b - T_{env}) + i_b^2 R_b + i_b T_b \frac{\partial V_{ocv}}{\partial T_b}, \quad (9)$$

where h and C_p are the heat transfer coefficient and the heat capacity of the battery, respectively [18], [20]. i_b (>0 on charge) and R_b are battery charge/discharge current and internal resistance, respectively; T_b is the battery temperature; T_{env} is the environmental temperature; $\partial V_{ocv}/\partial T_b$ is the entropic heat coefficient, which is a function of battery SOC, SOC_b. In (9) the first term represents the heat transferred to the environment; the second and third terms are irreversible heat generated from resistive dissipation $i_b^2 R_b$ and reversible entropic heat $i_b T_b \frac{\partial V_{ocv}}{\partial T_b}$, respectively. Here $\partial V_{ocv}/\partial T_b$ is experimentally measured at different SOC_b from 10% to 90% and listed in Table II.

Thus the temperature rise in battery ΔT_b under the pulsed current load can be expressed as

$$\Delta T_b = \frac{1}{C_p} \int_0^T \left[-h(T_b - T_{env}) + i_b^2 R_b + i_b T_b \frac{\partial V_{ocv}}{\partial T_b} \right] dt - T_{b,ini}, \quad (10)$$

where $T_{b,ini}$ is the initial temperature of the battery pack. ΔT_b in a specific system, battery-alone or hybrid ones, can

be calculated by using the actual battery current and internal resistance.

B. Passive HESS

In the passive HESS the battery and UC packs are directly connected in parallel, as shown in Fig. 1(b). C_{u1} and R_{u1} are the capacitance and internal resistance of the UC pack, respectively [21]. Based on the KVL and KCL (Kirchhoff's voltage and current laws) and Fig. 1(b), the following relationships can be obtained,

$$V_{o,b1} - i_{b,ps} R_{b1} = V_{o,u1} - i_{u,ps} R_{u1}, \quad (11)$$

$$i_{b,ps} = i_l - i_{u,ps}, \quad i_{u,ps} = -C_{u1} \frac{dV_{o,u1}}{dt}, \quad (12)$$

where $V_{o,b1}$, $V_{o,u1}$, $i_{b,ps}$, and $i_{u,ps}$ are the OCVs and currents of the battery and UC packs, respectively. Substituting $i_{b,ps}$ and $i_{u,ps}$, (12), into (11) gives

$$V_{o,u1} + \tau \frac{dV_{o,u1}}{dt} - V_{o,b1} + i_l R_{b1} = 0, \quad (13)$$

where the time constant τ is equal to $(R_{b1} + R_{u1})C_{u1}$ [22]. Since the purpose of the UC pack is to provide the dynamic current, it is reasonable to assume that $V_{o,u1}(0) = V_{o,u1}(T)$. Thus the differential equation, (13), can be solved to give $V_{o,u1}$, as shown in (14). The total energy from the battery

$$V_{o,u1} = \begin{cases} (I_{l,min} - I_{l,max})R_{b1} \frac{1 - e^{-\frac{DT}{\tau}}}{1 - e^{-\frac{T}{\tau}}} e^{-\frac{t}{\tau}} + V_{o,b1} - I_{l,min}R_{b1} & \text{if } 0 < t \leq (1 - D)T, \\ (I_{l,max} - I_{l,min})R_{b1} \frac{1 - e^{-\frac{(1-D)T}{\tau}}}{1 - e^{-\frac{T}{\tau}}} e^{-\frac{t-(1-D)T}{\tau}} + V_{o,b1} - I_{l,max}R_{b1} & \text{else,} \end{cases} \quad (14)$$

and UC packs, E_{total} , is calculated as

$$\begin{aligned} E_{total} &= \int_0^T i_{u,ps} V_{o,u1} dt + \int_0^T i_{b,ps} V_{o,b1} dt \\ &= - \int_0^T C_{u1} V_{o,u1} \frac{dV_{o,u1}}{dt} dt + \int_0^T (i_l - i_{u,ps}) V_{o,b1} dt \\ &= - \frac{C_{u1}}{2} [V_{o,u1}^2(T) - V_{o,u1}^2(0)] + V_{o,b1} I_{l,a} T \\ &\quad - V_{o,b1} \int_0^T i_{u,ps} dt = V_{o,b1} I_{l,a} T. \end{aligned} \quad (15)$$

Note that the integral of the UC current over period T , $\int_0^T i_{u,ps} dt$, is zero because $V_{o,u1}(0) = V_{o,u1}(T)$. The consumed energy of the load in the passive HESS is

$$\begin{aligned} E_{load} &= \int_0^T (V_{o,b1} - i_{b,ps} R_{b1}) i_l dt \\ &= \int_0^T V_{o,b1} i_l dt - \int_0^T (i_l - i_{u,ps}) i_l R_{b1} dt \\ &= V_{o,b1} I_{l,a} T - \int_0^T i_l^2 R_{b1} dt + \int_0^T i_{u,ps} i_l R_{b1} dt \\ &= V_{o,b1} I_{l,a} T - (I_{l,a}^2 + I_{l,dp} I_{l,dn}) R_{b1} T \\ &\quad + \int_0^T i_{u,ps} i_l R_{b1} dt. \end{aligned} \quad (16)$$

The third term, $\int_0^T i_{u,ps} i_l R_{b1} dt$, can be simplified as

$$\begin{aligned} \int_0^T i_{u,ps} i_l R_{b1} dt &= -C_{u1} R_{b1} \int_0^T \frac{dV_{o,u1}}{dt} i_l dt \\ &= -C_{u1} R_{b1} \left\{ I_{l,min} \int_0^{(1-D)T} \frac{dV_{o,u1}}{dt} dt \right. \\ &\quad \left. + I_{l,max} \int_{(1-D)T}^T \frac{dV_{o,u1}}{dt} dt \right\} \\ &= -C_{u1} R_{b1} \{ I_{l,min} [V_{o,u1}((1-D)T) - V_{o,u1}(0)] \\ &\quad + I_{l,max} [V_{o,u1}(T) - V_{o,u1}((1-D)T)] \} \\ &= \alpha I_{l,dp} I_{l,dn} R_{b1} T, \end{aligned}$$

where

$$\begin{aligned} \alpha &= \frac{R_{b1} (e^{Dk} - 1) [e^{(1-D)k} - 1]}{(R_{b1} + R_{u1}) D (1-D) k (e^k - 1)}, \\ k &= \frac{f_o}{f_l}, \quad f_o = \frac{1}{(R_{b1} + R_{u1}) C_{u1}}, \quad f_l = \frac{1}{T}. \end{aligned} \quad (17)$$

Here α is a term to represent the percentage of dynamic load current that is supplied by the UC pack. It is determined by the eigen-frequency of the passive HESS, f_o , and the frequency of the pulsed current load, f_l [22]. Thus the system efficiency of the passive HESS is

$$\begin{aligned} \eta_{ps} &= \frac{E_{load}}{E_{total}} = \frac{\int_0^T (V_{o,b1} - i_{b,ps} R_{b1}) i_l dt}{\int_0^T (V_{o,u1} i_{u,ps} + V_{o,b1} i_{b,ps}) dt} \\ &= \frac{V_{o,b1} I_{l,a} - I_{l,a}^2 R_{b1} - I_{l,dp} I_{l,dn} R_{b1} (1 - \alpha)}{V_{o,b1} I_{l,a}} \\ &= 1 - \frac{I_{l,a}^2 R_{b1} + I_{l,dp} I_{l,dn} R_p^*}{V_{o,b1} I_{l,a}}, \end{aligned} \quad (18)$$

where $R_p^* = R_{b1} (1 - \alpha)$.

C. Battery Semiactive HESS

In the battery semiactive HESS a dc-dc converter is placed between the battery pack and the load, as shown in Fig. 1(c). For the pulsed current load, the average load current is expected to be supplied by the battery pack with a high energy density, and the dynamic load current can be jointly provided by the battery and UC packs. Thus a current distribution coefficient, $C_{d,bs}$, can be defined as

$$C_{d,bs} \triangleq \frac{i_{d,bs} - I_{l,a}}{i_l - I_{l,a}}, \quad (19)$$

which is used to describe the percentage of the dynamic current that is provided by the battery pack through the dc-dc converter. Therefore, the currents of the dc-dc converter, the battery and UC packs are written as

$$i_{d,bs} = I_{l,a} + C_{d,bs} (i_l - I_{l,a}), \quad (20)$$

$$i_{u,bs} = (1 - C_{d,bs}) (i_l - I_{l,a}), \quad (21)$$

$$i_{b,bs} = \frac{V_{o,b2} - \sqrt{V_{o,b2}^2 - 4R_{b2} i_{d,bs} (V_{o,u1} - i_{u,bs} R_{u1})} \eta_d^{-s}}{2R_{b2}}, \quad (22)$$

where s is the sign of $i_{d,bs}$. Note the battery current, $i_{b,bs}$, is calculated considering the efficiency of the dc-dc converter, η_d . For the UC pack,

$$\frac{dV_{o,u1}}{dt} = \frac{-i_{u,bs}}{C_{u1}} = \frac{-(1 - C_{d,bs}) (i_l - I_{l,a})}{C_{u1}}, \quad (23)$$

i.e., a varying OCV of the UC pack. Then the system efficiency η_{bs} is expressed as

$$\eta_{bs} = \frac{\int_0^T (V_{o,u1} - i_{u,bs} R_{u1}) i_l dt}{\int_0^T (V_{o,u1} i_{u,bs} + V_{o,b2} i_{b,bs}) dt}, \quad (24)$$

which can be numerically calculated.

D. Capacitor Semiactive HESS

In the capacitor semiactive HESS the dc-dc converter is connected between the UC pack and the load, as shown in Fig. 1(d). Again $C_{d,cs}$ is defined to describe the percentage of the dynamic load current supplied by the battery pack. Similarly, the currents of the dc-dc converter, the battery and UC packs can be written as

$$i_{b,cs} = I_{l,a} + C_{d,cs} (i_l - I_{l,a}), \quad (25)$$

$$i_{d,cs} = (1 - C_{d,cs}) (i_l - I_{l,a}), \quad (26)$$

$$i_{u,cs} = \frac{V_{o,u2} - \sqrt{V_{o,u2}^2 - 4R_{u2} i_{d,cs} (V_{o,b1} - i_{b,cs} R_{b1})} \eta_d^{-s}}{2R_{u2}}, \quad (27)$$

where s is the sign of $i_{d,cs}$. The derivative of the OCV of the UC pack is given by

$$\frac{dV_{o,u2}}{dt} = \frac{-V_{o,u2} + \sqrt{V_{o,u2}^2 - 4R_{u2} i_{d,cs} (V_{o,b1} - i_{b,cs} R_{b1})} \eta_d^{-s}}{2R_{u2} C_{u2}}. \quad (28)$$

Thus the system efficiency η_{cs} can be expressed as

$$\eta_{cs} = \frac{\int_0^T (V_{o,b1} - i_{b,cs} R_{b1}) i_l dt}{\int_0^T (V_{o,u2} i_{u,cs} + V_{o,b1} i_{b,cs}) dt}. \quad (29)$$

III. SENSITIVITY ANALYSIS

Sensitivity analysis is performed below to quantitatively investigate the influences of the load profile and the system parameters on the energy efficiency and temperature rise in battery. Due to the nonlinearities of the previously derived efficiencies and temperature rises, the variation-based Sobol' method is applied for a global sensitivity analysis. The so-called Sobol' indices are used to quantify the amount of the variance that a single parameter or the correlation among parameters contributes to the total variance [23]. Five parameters, $I_{l,a}$, $I_{l,dp}$, $I_{l,dn}$, SOC_b , and η_d , are selected to investigate the relative importances of an individual parameter and pairs of them. These two criteria are represented by the first and second order Sobol' indices, respectively. The ranges of the parameters in the sensitivity analysis are shown in Table III and the distributions of the parameters are assumed to be uniform. $I_{l,a}$, $I_{l,dp}$, and $I_{l,dn}$ are the three parameters to define a pulsed current load [see Fig. 2]. The quasi-Monte Carlo algorithm with quasi-random samples, one million Halton points, is adopted to estimate the first and second order Sobol' indices. The quasi-Monte Carlo algorithm is known to have a faster convergence than the conventional Monte Carlo algorithm [24].

TABLE III
RANGES OF PARAMETERS.

Parameter	$I_{l,a}$	$I_{l,dp}$	$I_{l,dn}$	SOC_b	η_d
Min	1 A	1 A	1 A	0.1	0.9
Max	5 A	5 A	5 A	0.9	1.0

TABLE IV
CONNECTIONS OF BATTERY AND UC CELLS.

Topology	Bat.-alone	Passive	Bat. Semi.	Cap. Semi.
Bat. Pack	4S2P	4S2P	2S4P	4S2P
UC Pack	N/A	8S1P	8S1P	4S2P

In the following analysis eight lithium-ion battery cells are connected in 4S2P (4 series 2 parallel) for the battery-alone system. The size and connection of the UC pack is determined to enable a similar dc bus voltage variation with the battery-alone system. The battery semiactive HESS has the largest dc bus voltage variation since the battery pack is decoupled from the load. Thus this HESS is selected to determine the size of the UC pack at 50% SOC_b . Its maximum variation of the dc bus voltage over the period T ($=10$ s) is reached when $C_{d,bs}$ is zero [refer to (23)],

$$\Delta V_{bus,max} = (I_{l,max} - I_{l,min}) \left[R_{u1} + \frac{D(1-D)T}{C_{u1}} \right]. \quad (30)$$

Therefore the size of the UC pack should satisfy

$$R_{u1} + \frac{D(1-D)T}{C_{u1}} \approx R_{b1}, \quad (31)$$

which requires an 8S1P connection, as shown in Table I. The battery cells are then connected in 2S4P to have a nearly

50% duty cycle of the dc-dc converter. The connections in the other two HESSs are similarly determined and summarized in Table IV. Note that the current ripple of a real dc-dc converter may affect the performances of the two semiactive HESSs. Existing literature shows that when the peak-to-peak ripple of the battery current is nearly 200% of its dc component, about 15% additional heat is generated [25]. Taking the battery semiactive HESS in the experiments as an example, with a 50% duty cycle of the dc-dc converter and a 50% SOC_b , the peak-to-peak ripple of the battery current is $\frac{d_s V_{o,b2}}{L f_s} = 0.76$ A. The parameters d_s ($=50\%$), L ($=250 \mu\text{H}$), and f_s ($=20$ kHz) are the duty cycle, inductance of the inductor, and switching frequency of the dc-dc converter, respectively. In the worst case, i.e., the smallest average load current $I_{l,a}$ ($=1$ A) in Table III, the above peak-to-peak battery current is only 38% of the dc component, 2 A, considering the 50% duty cycle of the dc-dc converter. Thus the influence of the current ripple of the dc-dc converter is neglected in the following analysis.

A. System efficiency

The current distributions, $C_{d,bs}$ and $C_{d,cs}$, are first optimized to maximize the system efficiencies of the battery and capacitor semiactive HESSs, respectively [refer to section II-C and D]. The expectation and standard deviation of the system efficiencies for the one million samples, $\hat{E}(y)$ and $\hat{\sigma}(y)$, are shown in Table V. It can be seen that due to the lack of the dc-dc converter, the passive HESS is the most efficient system and its efficiency is the least sensitive to the variations of the parameters. Meanwhile, as discussed below, compared with the two semiactive HESSs, the passive HESS is sensitive to the characteristics of the load profile. In addition, the uncontrolled current distribution between the battery and UC packs make the passive HESS less attractive [8]. With one dc-dc converter, the capacitor semiactive HESS is averagely more efficient than the battery semiactive HESS. Note the average efficiency of the battery semiactive HESS is actually lower than that of the battery-alone system, but it significantly improves the robustness of the system efficiency against variations of the dynamic current in the load profile, as shown in the following Sobol' indices-based analysis.

TABLE V
EXPECTATION AND STANDARD DEVIATION OF EFFICIENCIES.

Topology	Battery-alone	Passive	Bat. Semi.	Cap. Semi.
$\hat{E}(y)$	0.8980	0.9419	0.8897	0.9146
$\hat{\sigma}(y)$	0.0377	0.0150	0.0335	0.0265

Figs. 3 and 4 show the first and second order Sobol' indices representing the relative importances of an individual parameter and the pairs. For the battery-alone system and the passive HESS, they are both sensitive to the characteristics of the load profile, i.e., $I_{l,a}$, $I_{l,dp}$, and $I_{l,dn}$. Meanwhile, with the high-efficiency UC pack the passive HESS is less sensitive to the characteristics of the dynamic load current, i.e., $I_{l,dp}$ and $I_{l,dn}$, but more sensitive to the average load current, $I_{l,a}$. It is interesting to note that the efficiency of the battery semiactive HESS highly depends on the efficiency of

the dc-dc converter, η_d ; while the capacitor semiactive HESS is sensitive to the dynamic load current, i.e., $I_{l,dp}$ and $I_{l,dn}$. At the same time, parameter correlations in Fig. 4 show that the battery semiactive HESS is a relatively straightforward HESS, in which the efficiency of the dc-dc converter is a dominant factor. However, the behavior of the capacitor semiactive HESS is complicated due to the strong correlations among the parameters. The results of the above efficiency analysis provide a basis for choosing a proper HESS topology that best fits a target application.

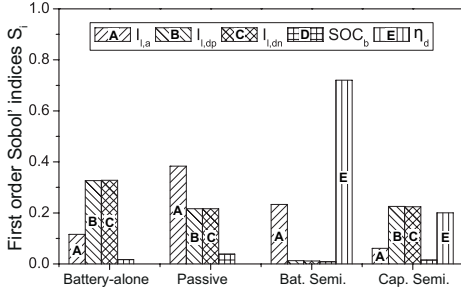


Fig. 3. First order Sobol' indices for system efficiencies.

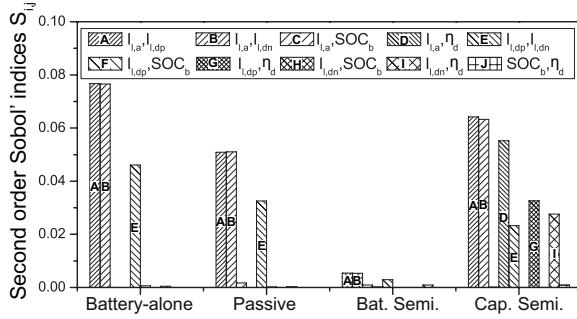


Fig. 4. Second order Sobol' indices for system efficiencies.

B. Temperature rise in battery

Again the current distributions $C_{d,bs}$ and $C_{d,cs}$ are optimized to minimize ΔT_b in the battery and capacitor semiactive HESSs, respectively. The expectation and standard deviation of ΔT_b in a single period of the load profile, 10 s, are shown in Table VI for the one million samples. It shows that the battery temperature rise in the capacitor semiactive HESS $\Delta T_{b,cs}$ is the lowest on average and is the least sensitive to the system parameters and load profile. The battery-alone system has the highest average ΔT_b . Combining the UCs the temperature rise in battery can be effectively reduced, which would lead to an extended battery cycle life.

TABLE VI

EXPECTATION AND STANDARD DEVIATION OF TEMPERATURE RISES.

Topology	Battery-alone	Passive	Bat. Semi.	Cap. Semi.
$\hat{E}(y)$ [°C]	0.2062	0.1368	0.1621	0.1309
$\hat{\sigma}(y)$ [°C]	0.0943	0.0833	0.1074	0.0830

Figs. 5 and 6 show the first and second order Sobol' indices for analyzing the temperature rise in battery. Quite

different with the system efficiencies, all the temperature rises in the four systems mostly depend on the average load current $I_{l,a}$ and the battery SOC SOC_b . This is because the irreversible resistive heat is affected by $I_{l,a}$, $I_{l,dp}$, and $I_{l,dn}$, while the reversible entropic heat generated over the single period mainly depends on $I_{l,a}$, i.e., the term of the integration of i_b in (10). Thus $I_{l,a}$ has a larger influence on the temperature rise than $I_{l,dp}$ and $I_{l,dn}$. Meanwhile, SOC_b influences both the irreversible resistive and reversible entropic heats. With the UC pack to supply the dynamic load current, the battery temperature rises in the three battery-UC HESSs are insensitive to the dynamic component of the load profile, i.e., $I_{l,dp}$ and $I_{l,dn}$. Again a strong correlation between $I_{l,a}$ and SOC_b is observed in all the three HESSs, as shown in Fig. 6. Note the influence of η_d is only obvious in the battery semiactive HESS because the dc-dc converter is directly connected with the battery pack. In terms of the protection of the battery, the capacitor semiactive HESS is the best among the three battery-UC HESSs.

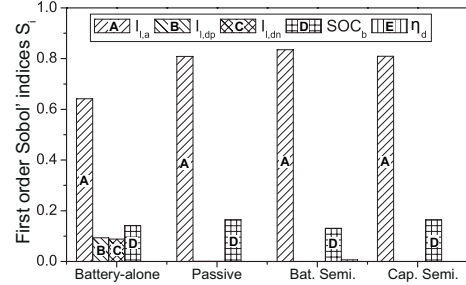


Fig. 5. First order Sobol' indices for temperature rises in battery.

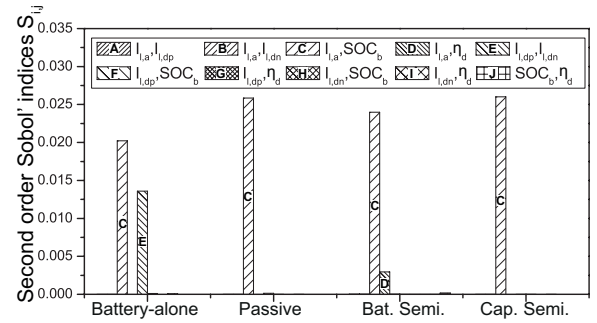


Fig. 6. Second order Sobol' indices for temperature rises in battery.

IV. PROPER USAGE OF HESSs

Thanks to the above sensitivity analysis, the proper usage of the HESSs can be quantitatively discussed considering the most influential factors. Since the sensitivities of $I_{l,dp}$ and $I_{l,dn}$, i.e., the two parameters representing the dynamic load current, are close in all the above cases, for the sake of simplicity $I_{l,dn}$ is set to be equal to $I_{l,dp}$ in the following discussions. The below results in Figs. 7–10 are obtained through numerical simulation.

A. System efficiency

Merely in terms of efficiency, the simple passive HESS is the best. However, it is sensitive to the characteristics of

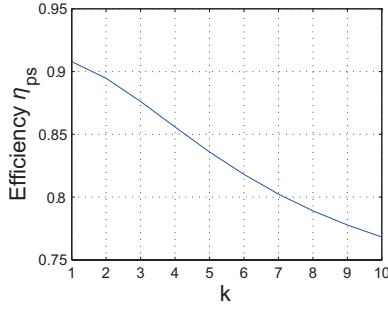


Fig. 7. System efficiency of the passive HESS, η_{ps} , versus k ($=f_o/f_i$) when $I_{l,a} = 1$ A, $I_{l,dp} = I_{l,dn} = 5$ A [refer to (17)].

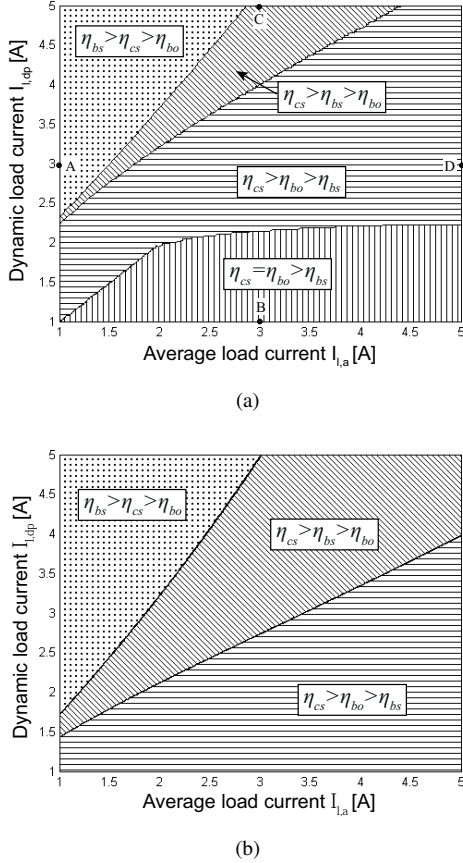


Fig. 8. System efficiencies of battery-alone system, battery semiactive HESS, and capacitor semiactive HESS ($\text{SOC}_b = 50\%$). (a) $\eta_d = 95\%$. (b) $\eta_d = 98\%$.

the load profile, particularly the load frequency. For example, the efficiency of the passive HESS significantly drops as the frequency of the pulsed current load becomes lower than its eigen-frequency [refer to Fig. 7, (17), and (18)], while the efficiencies of the other three systems are irrelevant to the frequency of the load [refer to (8), (24), and (29)]. It is known that the uncontrollable current flow in the passive HESS also causes low UC utilization (39.5% in the current configuration) and adversely affects the battery cycle life [8], [26]. These drawbacks limit the application of the passive HESS. The passive HESS mainly serves as a reference in the following sections.

Thus the efficiencies of the battery-alone system, battery and capacitor semiactive HESSs are discussed below. Fig. 8(a)

and (b) graphically compare the efficiencies versus average load current $I_{l,a}$ and dynamic load current $I_{l,dp}(=I_{l,dn})$ at 95% and 98% efficiencies of the dc-dc converter η_d . The two subfigures show that efficiency of the battery semiactive HESS η_{bs} is the highest when the load profile has a small $I_{l,a}$ and large $I_{l,dp}$, namely a highly dynamic load profile. Except in this region, the capacitor semiactive HESS is always the most efficient. Meanwhile, under a relatively smooth load profile, i.e., with a small $I_{l,dp}$, the two semiactive battery-UC HESSs may not be advantageous, particularly when efficiency of the dc-dc converter is relatively low. In this case the battery-alone system itself is already sufficiently efficient [see Fig. 8(a)]. A high-efficiency dc-dc converter is important to justify the usage of the semiactive battery-UC HESSs. The battery semiactive HESS is superior under a strong dynamic load, while generally the capacitor semiactive HESS is more efficient in other cases.

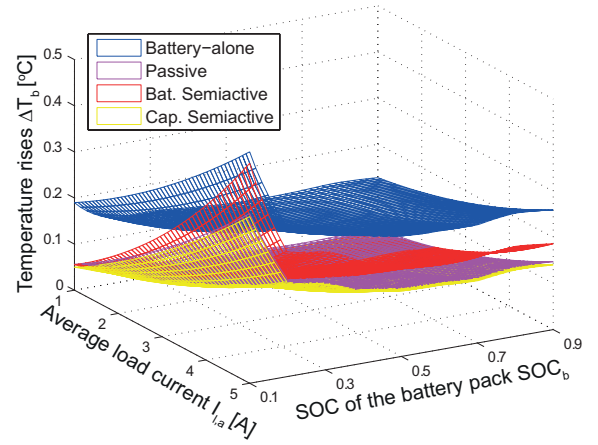


Fig. 9. Battery temperature rises in battery-alone system, passive HESS, battery and capacitor semiactive HESSs ($I_{l,dp} = 5$ A, $\eta_d = 95\%$).

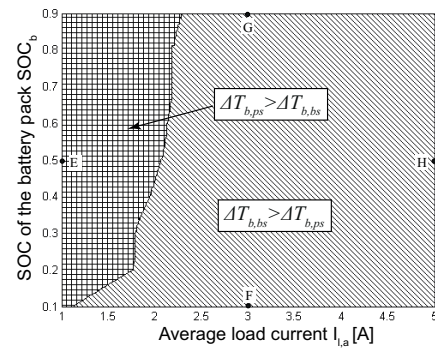


Fig. 10. Battery temperature rises in passive HESS and battery semiactive HESS ($I_{l,dp} = 5$ A, $\eta_d = 95\%$).

B. Temperature rise in battery

Fig. 9 shows the temperature rises in battery ΔT_b versus the two most influential parameters, average load current $I_{l,a}$ and SOC of the battery pack SOC_b , during a single period of the pulsed load profile, 10 s. The temperature rise in the conventional battery-alone system is the highest. All maximum ΔT_b 's

are reached when SOC_b is 10% and $I_{l,a}$ is 5 A. It is because the absolute value of the entropic heat coefficient $\partial V_{ocv}/\partial T_b$ is the largest at the low 10% SOC_b and the heat generated from the resistive dissipation increases with an increasing $I_{l,a}$. The temperature rise ΔT_b in the capacitor semiactive HESS is always the lowest. In this HESS the optimized $C_{d,cs}$ is zero [refer to section II-D]. Thus the battery pack only supplies the average load current. For reference purposes, $\Delta T_{b,ps}$ and $\Delta T_{b,bs}$, the respective battery temperature rises in the passive and battery semiactive HESSs, under different $I_{l,a}$ and SOC_b are graphically compared in Fig. 10. It is interesting to note that as same as in the previous analysis of efficiency, the battery semiactive HESS is superior when the pulsed load profile is highly dynamic, i.e., a small average load current $I_{l,a}$ here. Meanwhile, when $I_{l,a}$ increases, the voltage drop of the battery caused by its internal resistance increases. It in turn leads to a larger battery current to maintain a nearly constant output power of the dc-dc converter, and thus higher ΔT_b than that in the passive HESS. Again a high-efficiency dc-dc converter helps to reduce the temperature rise in the battery pack.

V. EXPERIMENTAL VALIDATION

The experimental setup is shown in Fig. 11 taking the capacitor semiactive HESS as an example. The setup was reconfigured to also emulate passive and battery semiactive HESSs, and battery-alone system. As shown in the figure, the power supply and the electronic load are combined together to emulate the charging and discharging currents (i_{ch} and i_{dis}). The buck-boost bidirectional dc-dc converter was designed and fabricated in house. The pulse width modulation (PWM) control of the output current of the dc-dc converter is performed by using the National Instruments (NI) compactRIO. The NI CompactRIO also collects data such as battery voltage (V_b), battery temperature (T_b), UC voltage/current (V_u and $i_{u,cs}$), output current of the dc-dc converter ($i_{d,cs}$), load current (i_l), and environmental temperature (T_{env}). Three 0.01Ω high-accuracy sampling resistors, R_{s1} , R_{s2} , and R_{s3} , are used to measure the currents of the dc-dc converter, UC pack, and load, respectively. The battery current is equal to the difference between the currents of the load and the dc-dc converter. Two T-type thermocouples are used to measure the battery and environmental temperatures. The specifications of the experimental setup are summarized in Table VII.

There are many topologies for the dc-dc converters. Thus for generality, in the above analysis the constant efficiencies, 95% and 98%, are used for the dc-dc converter, which are reasonable for today's power electronic devices. For verification purposes, the power loss of the specific dc-dc converter in the experimental setup is calculated as follows [see Fig. 12] [27].

$$P_{loss,d} = i_L^2(R_{mos} + R_L) + 2V_d Q_g f_s, \quad (32)$$

where R_{mos} ($=15\text{ m}\Omega$), R_L ($=20\text{ m}\Omega$) are resistances of the MOSFET and the inductor, respectively; V_d ($=15\text{ V}$) is the gate drive voltage; Q_g ($=92\text{ nC}$) is the gate charge of the MOSFET; f_s ($=20\text{ kHz}$) is the switching frequency; i_L is the current of the inductor. As shown in Fig. 13, the relationships among

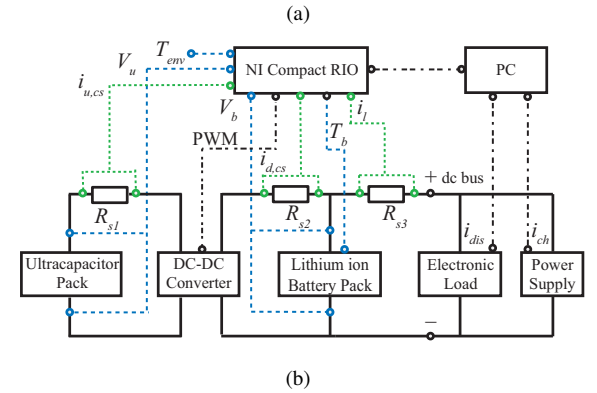
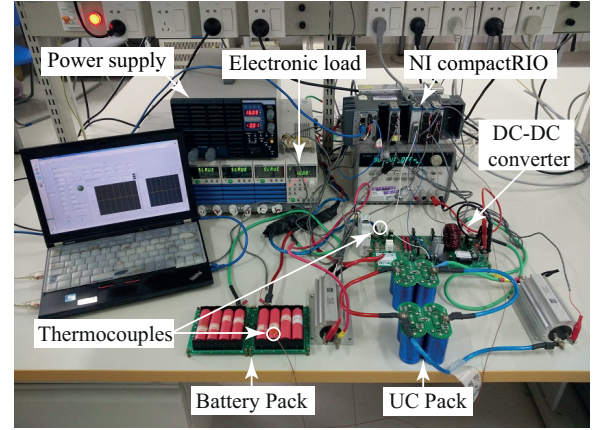


Fig. 11. An example of the experimental setup (capacitor semiactive HESS). (a) Photo. (b) Blockdiagram.

TABLE VII
SPECIFICATIONS FOR MAJOR COMPONENTS.

Battery Pack (Sanyo 18650 Li-ion battery)	8 cells (2S4P and 4S2P) 2.5 Ah/cell, 3.7 V/cell (Nom. Vol.)
UC Pack (Samwha DB series)	8 cells (8S1P and 4S2P) 500 F/cell, 2.7 V/cell (Max Vol.)
Power Supply (Takasago ZX-800L)	Max Power: 800 W 0–80 V, 0–80 A
Electronic Load (Kikusui PLZ-50F/150U)	Max Power: 600 W 1.5–150 V, 0–120 A
DC-DC Converter (Design/fabricate in house)	Max Power: 400 W Average Efficiency: 95%
Sampling Resistors (PCN Corporation RH series)	Three RH250M4: 0.01 Ω Accuracy: $\pm 0.02\%$
Thermocouples (Fluke TT-T-30)	Insulation range: -267 – $260\text{ }^\circ\text{C}$
Control and DAQ System (NI compactRIO)	I/O board: NI 9401 A/D boards: NI 9219 $\times 2$, NI 9203

the efficiencies are as same as the results in Fig. 8(a) using a constant 95% efficiency of the dc-dc converter. Note that the average efficiency of the real dc-dc converter is 95%.

The system efficiencies of the four systems, the battery-alone system, passive HESS, battery and capacitor semiactive HESSs, were measured and shown in Fig. 15 under the different combinations of average load current $I_{l,a}$ and dynamic load current $I_{l,dp}$ at points A to D in Fig. 8(a). The pulsed

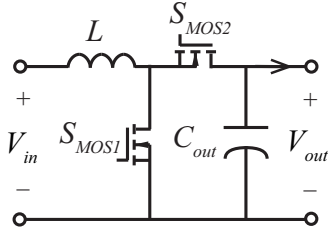


Fig. 12. Schematic of the dc-dc converter.

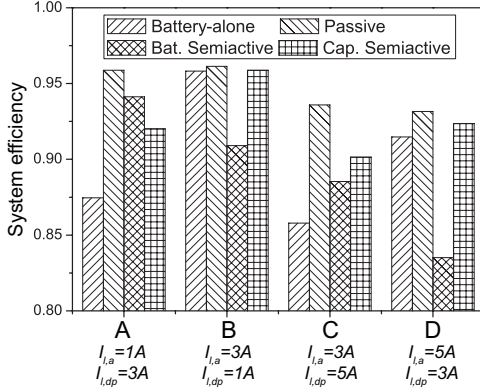


Fig. 13. Calculated efficiencies of the four systems at points A to D in Fig. 8(a) using the loss model of the dc-dc converter in (32).

current load profiles at points A–D are shown in Fig. 14. Relationships among the system efficiencies well match with the previous calculation results. The figure clearly shows the benefit of the hybridization with UCs, particularly under a small $I_{l,a}$ and a large $I_{l,dp}$ (such as at point A). Between the two semiactive HESSs, the efficiency of the battery semiactive HESS is more sensitive to the average load current, as shown by the efficiencies at points A and D. This drop in efficiency is mainly caused by the increased energy loss in the dc-dc converter in the battery semiactive HESS. The efficiency map in Fig. 8 can serve as a guideline when choosing a proper HESS topology for a target load dynamics.

Similarly, the temperature rises in the battery pack were measured and shown in Fig. 17 under the combinations of average load current $I_{l,a}$ and SOC of the battery pack SOC_b at points E to H in Fig. 10. The pulsed current load profiles at points E–H are shown in Fig. 16. In the profiles, the dynamic current is maximized ($I_{l,dp}=I_{l,dn}=5$ A) in order to clearly observe the temperature rises. Note that the two profiles at points F and G are identical but with different SOC_b . In the experiments, the pulsed current load is repeated until 5% reduction of the capacity is reached when starting from 50% and 90% SOC_b . For the low 10% SOC_b , in order to prevent the overdischarge of the battery the pulsed current load is repeated until the voltage of the battery pack drops to 10 V. Fig. 17 shows that the temperature rises in battery are reduced in all the three battery-UC HESSs. As same as in the previous theoretical discussions, in terms of the reduction of the temperature rise in battery, i.e., the protection of battery, the capacitor semiactive HESS is more advantageous than the battery semiactive HESS, particularly when the average load

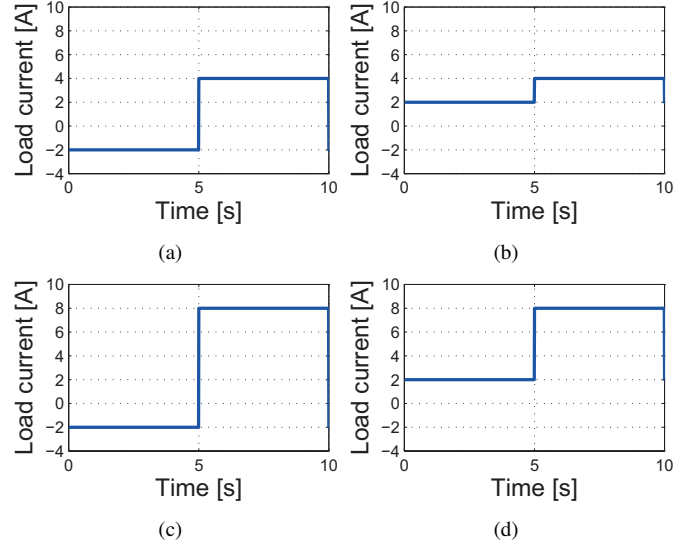


Fig. 14. Pulsed current load profiles at points A to D. (a) Point A. (b) Point B. (c) Point C. (d) Point D.

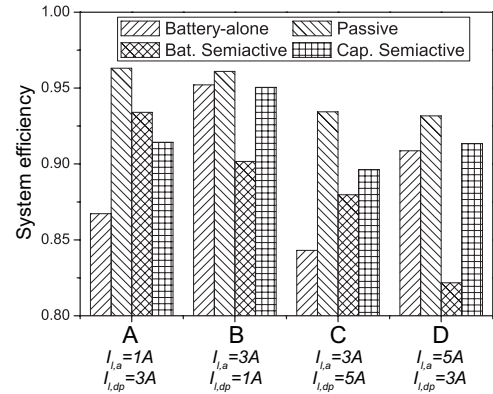


Fig. 15. System efficiencies of the four systems at points A to D in Fig. 8(a).

current $I_{l,a}$ is large [refer to point H in Fig. 10].

For reference purposes, a realistic current load profile from the Japanese JC08 cycle is used to investigate the performances of the four systems. The JC08 cycle was designed to represent a congested city driving [28]. Table VIII shows system efficiencies (η_{sys}) and battery temperature rises in experiments under the JC08 profile. The results are consistent with those of the above quantitative analysis using the pulsed current load profiles. Under the highly dynamic JC08 profile, the battery semiactive HESS is superior in terms of system efficiency, while the capacitor semiactive HESS better suppresses the battery temperature rise. Thus the above analysis using the pulsed current load profiles provides general guidelines for the selection of a proper battery-UC HESS in real applications.

TABLE VIII
EXPERIMENTAL RESULTS UNDER THE REALISTIC JC08 CURRENT PROFILE.

Topology	Battery-alone	Passive	Bat. Semi.	Cap. Semi.
η_{sys}	0.884	0.937	0.930	0.923
ΔT_b	3.32	1.82	1.08	0.73

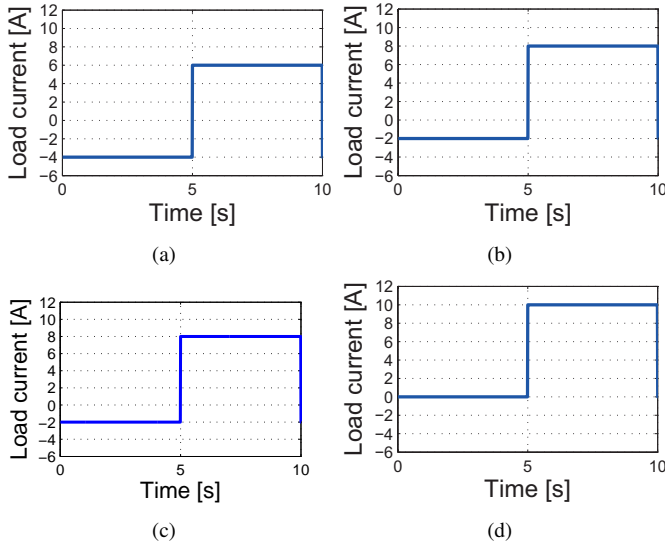


Fig. 16. Pulsed current load profiles at points E to H. (a) Point E. (b) Point F. (c) Point G. (d) Point H.

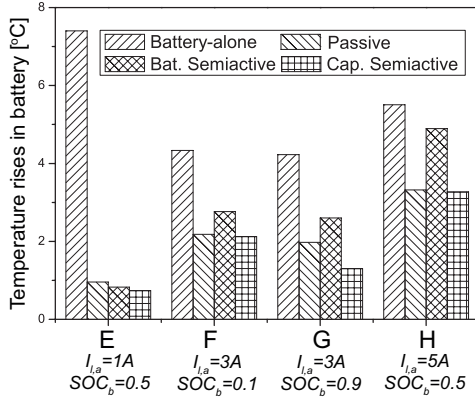


Fig. 17. Battery temperature rises in the four systems at points E to H in Fig. 10.

VI. ADDITIONAL DISCUSSIONS ON COST METRIC

Besides the technical aspects, the cost metric of the above four systems (e.g., volume, mass, economic cost) is discussed as follows. Note that the passive HESS is included for reference purposes. As discussed above, the drawbacks of the passive HESS limit its application. When comparing competing systems, there is usually a tradeoff between improved performance and added complexity, cost, volume, mass, etc. The above analysis quantitatively investigates the performances of the battery-alone system, passive HESS, battery and capacitor semiactive HESSs in terms of the energy efficiency and temperature rise in battery. The below discussions on the cost metric help to further address the complicated tradeoff relationships when designing a practical energy storage system.

From [15], [29], the cost, mass, and volume of the dc-dc converter are assumed to be 50 USD kW^{-1} , 0.19 kg kW^{-1} , 0.18 L kW^{-1} . The estimated cost of lithium-ion battery and UC are supposed as about 1500 USD kWh^{-1} and 15000 USD kWh^{-1} , respectively [30], [31]. The cost, mass, and vol-

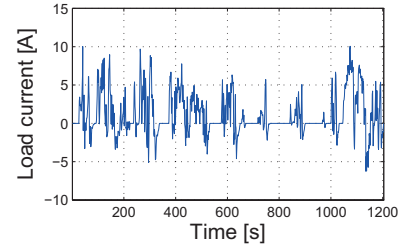


Fig. 18. Realistic JC08 current load profile.

ume of the four systems are calculated taking the experimental setup in Fig. 11 as an example, and listed in Table IX. Note that as shown in Table IV, the numbers of the battery and UC cells are same in the battery and capacitor semiactive HESSs.

TABLE IX
COST, MASS, AND VOLUME OF FOUR SYSTEMS.

Topology	Battery-alone	Passive	Bat. Semi.	Cap. Semi.
Cost [USD]	111	171	191	191
Mass [kg]	0.344	0.904	0.980	0.980
Volume [L]	0.136	0.600	0.672	0.672

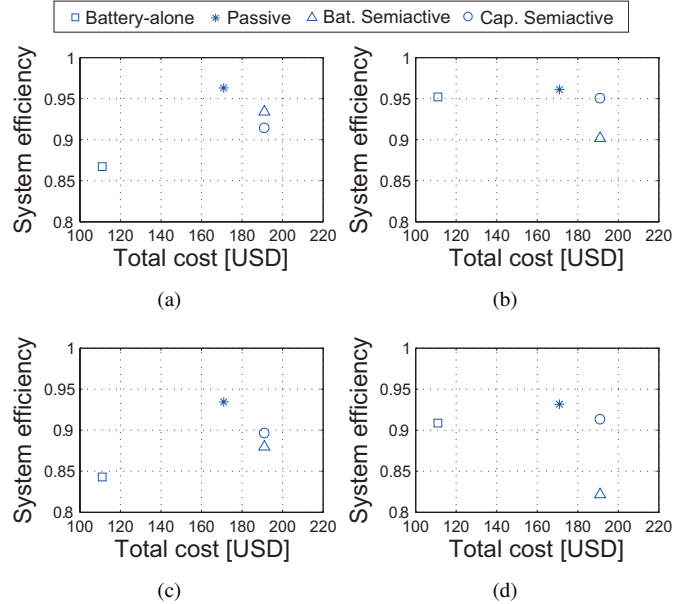


Fig. 19. System efficiencies versus costs at points A to D. (a) Point A. (b) Point B. (c) Point C. (d) Point D.

Fig. 19 illustrates the tradeoff relationship between system efficiencies of the four systems and their costs at points A–D in Fig. 8(a). Again, compared with the battery-alone system, the two semiactive HESSs show better cost performance at points A and C, i.e., highly dynamic loads. In the current example, the cost is 12–15 USD for 1% efficiency improvement when using the semiactive HESSs. The HESSs are less cost-effective at points B and D, i.e., smooth loads, because the efficiency of the battery-alone system is already over 90%. Similarly, Fig. 20 shows the battery temperature rises versus the costs at

points E–H in Fig. 10. At point E, i.e., the most dynamic load, the semiactive HESSs show the largest reduction of the battery temperature rise. For the current example, the cost is 12 USD for 1 °C reduction of battery temperature rise. As shown in Table IX, the mass and volume of the battery-UC HESSs are about 1.5 times and 3.0 times larger than those of the battery-alone system, respectively. Currently, the battery-UC HESSs are considered suitable for applications in utility grids and larger vehicles such as buses. These applications are less restrictive on weight, volume, and cost. New technologies and mass production are expected to further improve the energy density and cost-effectiveness of the UCs, i.e., smaller, lighter, and cheaper UC cells.

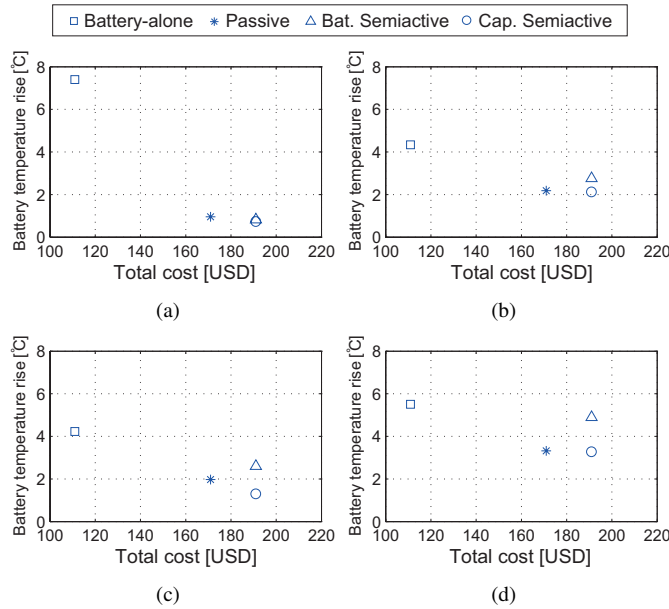


Fig. 20. Battery temperature rises versus costs at points E to H. (a) Point E. (b) Point F. (c) Point G. (d) Point H.

VII. CONCLUSIONS

In this paper the system efficiencies and the battery temperature rises in the battery-alone system and the three representative battery-UC HESSs are derived under a pulsed current load. Sensitivity analysis is then performed to investigate the influences of the characteristics of the load profiles, the state of charge of batteries, and the efficiency of the dc-dc converter on the four energy storage systems. The proper usage of the HESSs is discussed later based on the results of the sensitivity analysis. The drawbacks such as the dependence on the load frequency limit the application of the passive HESS. It is found that the capacitor semiactive HESS is advantageous in terms of efficiency. However, compared with the battery semiactive HESS its efficiency is more sensitive to the load dynamics, and the strong correlations among the parameters make its behavior complicated. Meanwhile, the battery semiactive HESS is a relatively straightforward HESS and efficient when the load is highly dynamic. At the same time, the efficiency of the battery semiactive HESS significantly depends on the efficiency of the dc-dc converter.

The hybridization with the UCs makes the battery temperature rise in the HESSs less sensitive to the dynamic component of the load. The capacitor semiactive HESS shows the best performance in suppressing the temperature rise in battery (i.e., protection of battery). The improvement in the temperature rise is obvious in the battery semiactive HESS when the load becomes more dynamic. Again this improvement is sensitive to the efficiency of the dc-dc converter. The above results provide guidelines for the proper usage of the battery-UC HESSs in the applications with different load dynamics. Considering the cost metric (e.g., volume, mass, economic cost), currently the battery-UC HESSs are suitable for applications such as utility grids and larger vehicles. Improvements in technology and mass production are expected to further expand their applications. The systematic approach developed in this paper can be used to discuss other factors in the battery-UC HESSs, and further extended to discuss more HESS topologies.

REFERENCES

- [1] P. Nema, R. Nema, and S. Rangnekar, "A current and future state of art development of hybrid energy system using wind and PV-solar: A review," *Renewable and Sustainable Energy Rev.*, vol. 13, no. 8, pp. 2096–2103, 2009.
- [2] C. Hill, M. C. Such, D. Chen, J. Gonzalez, W. M. Grady *et al.*, "Battery energy storage for enabling integration of distributed solar power generation," *IEEE Trans. Smart Grid*, vol. 3, no. 2, pp. 850–857, 2012.
- [3] J. Cao and A. Emadi, "A new battery/ultracapacitor hybrid energy storage system for electric, hybrid, and plug-in hybrid electric vehicles," *IEEE Trans. Power Electron.*, vol. 27, pp. 122–132, Jan. 2012.
- [4] X. Hu, N. Murgovski, L. M. Johannesson, and B. Egardt, "Comparison of three electrochemical energy buffers applied to a hybrid bus powertrain with simultaneous optimal sizing and energy management," *IEEE Trans. Intell. Transp. Syst.*, vol. 15, no. 3, pp. 1193–1205, 2014.
- [5] A. Burke and M. Miller, "The power capability of ultracapacitors and lithium batteries for electric and hybrid vehicle applications," *J. Power Sources*, vol. 196, no. 1, pp. 514–522, 2011.
- [6] A. Burke, "Ultracapacitors: why, how, and where is the technology," *J. Power Sources*, vol. 91, no. 1, pp. 37–50, 2000.
- [7] S. Vazquez, S. M. Lukic, E. Galvan, L. G. Franquelo, and J. M. Carrasco, "Energy storage systems for transport and grid applications," *IEEE Trans. Ind. Electron.*, vol. 57, no. 12, pp. 3881–3895, 2010.
- [8] I. Aharon and A. Kuperman, "Topological overview of powertrains for battery-powered vehicles with range extenders," *IEEE Trans. Power Electron.*, vol. 26, no. 3, pp. 868–876, 2011.
- [9] G. Sikha and B. N. Popov, "Performance optimization of a battery-capacitor hybrid system," *J. Power Sources*, vol. 134, pp. 130–138, Jul. 2004.
- [10] L. Gao, R. A. Dougal, and S. Liu, "Power enhancement of an actively controlled battery/ultracapacitor hybrid," *IEEE Trans. Power Electron.*, vol. 20, pp. 236–243, Jan. 2005.
- [11] J. C. Schroeder and F. W. Fuchs, "General analysis and design guideline for a battery buffer system with dc/dc converter and EDLC for electric vehicles and its influence on efficiency," *IEEE Trans. Power Electron.*, vol. 30, no. 2, pp. 922–932, 2015.
- [12] R. Carter, A. Cruden, and P. J. Hall, "Optimizing for efficiency or battery life in a battery/supercapacitor electric vehicle," *IEEE Trans. Veh. Technol.*, vol. 61, no. 4, pp. 1526–1533, 2012.
- [13] J. M. Blanes, R. Gutierrez, A. Garrigós, J. L. Lizán, and J. M. Cuadrado, "Electric vehicle battery life extension using ultracapacitors and an FPGA controlled interleaved buck-boost converter," *IEEE Trans. Power Electron.*, vol. 28, no. 12, pp. 5940–5948, 2013.
- [14] J. Moreno, M. E. Ortúzar, and J. W. Dixon, "Energy-management system for a hybrid electric vehicle, using ultracapacitors and neural networks," *IEEE Trans. Ind. Electron.*, vol. 53, pp. 614–623, Apr. 2006.
- [15] J. Dixon, I. Nakashima, E. F. Arcos, and M. Ortúzar, "Electric vehicle using a combination of ultracapacitors and ZEBRA battery," *IEEE Trans. Ind. Electron.*, vol. 57, no. 3, pp. 943–949, 2010.

- [16] J. Wang, P. Liu, J. Hicks-Garner, E. Sherman, S. Soukiazian, M. Verbrugge, H. Tataria, J. Musser, and P. Finamore, "Cycle-life model for graphite-LiFePO₄ cells," *J. Power Sources*, vol. 196, no. 8, pp. 3942–3948, 2011.
- [17] C. Zhao, H. Yin, Z. Yang, and C. Ma, "Equivalent series resistance-based energy loss analysis of a battery semiactive hybrid energy storage system," *IEEE Trans. Energy Convers.*, vol. 30, no. 3, pp. 1081–1091, 2015.
- [18] R. Richardson and D. Howey, "Sensorless battery internal temperature estimation using a kalman filter with impedance measurement," *IEEE Trans. Sustain. Energy*, vol. 6, no. 4, pp. 1190–1199, 2015.
- [19] R. C. Kroeze and P. T. Krein, "Electrical battery model for use in dynamic electric vehicle simulations," in *Proc. IEEE Power Electronics Specialists (PESC'2008)*, Rhodes, Greece, Jun. 2008, pp. 1336–1342.
- [20] C. Forgez, D. V. Do, G. Friedrich, M. Morcrette, and C. Delacourt, "Thermal modeling of a cylindrical LiFePO₄/graphite lithium-ion battery," *J. Power Sources*, vol. 195, no. 9, pp. 2961–2968, 2010.
- [21] Z. Song, H. Hofmann, J. Li, X. Han, X. Zhang, and M. Ouyang, "A comparison study of different semi-active hybrid energy storage system topologies for electric vehicles," *J. Power Sources*, vol. 274, pp. 400–411, 2015.
- [22] R. A. Dougal, S. Liu, and R. E. White, "Power and life extension of battery-ultracapacitor hybrids," *IEEE Trans. Compon. Packag. Technol.*, vol. 25, pp. 120–131, Mar. 2002.
- [23] I. M. Sobol', "Global sensitivity indices for nonlinear mathematical models and their monte carlo estimates," *Mathematics and computers in simulation*, vol. 55, no. 1, pp. 271–280, 2001.
- [24] —, "On quasi-monte carlo integrations," *Mathematics and Computers in Simulation*, vol. 47, no. 2, pp. 103–112, 1998.
- [25] S. Bala, T. Tegnér, P. Rosenfeld, and F. Delince, "The effect of low frequency current ripple on the performance of a lithium iron phosphate (LFP) battery energy storage system," in *Proc. IEEE Energy Convers. Congr. Expo.*, 2012, pp. 3485–3492.
- [26] R. Chandrasekaran, G. Sikha, and B. N. Popov, "Capacity fade analysis of a battery/super capacitor hybrid and a battery under pulse loads—full cell studies," *Journal of applied electrochemistry*, vol. 35, no. 10, pp. 1005–1013, 2005.
- [27] Y. Choi, N. Chang, and T. Kim, "DC-DC converter-aware power management for low-power embedded systems," *IEEE Trans. Comput.-Aid. Des.*, vol. 26, pp. 1367–1381, Aug. 2007.
- [28] S. Chopra and P. Bauer, "Driving range extension of EV with on-road contactless power transfer-a case study," *IEEE Trans. Ind. Electron.*, vol. 60, no. 1, pp. 329–338, 2013.
- [29] T. A. Burress, S. L. Campbell, C. Coomer, C. W. Ayers, A. A. Wereszczak, J. P. Cunningham, L. D. Marlino, L. E. Seiber, and H.-T. Lin, "Evaluation of the 2010 toyota prius hybrid synergy drive system," Power Electronics and Electric Machinery Research Facility, Oak Ridge National Laboratory (ORNL), Tech. Rep., 2011.
- [30] R. T. Doucette and M. D. McCulloch, "A comparison of high-speed flywheels, batteries, and ultracapacitors on the bases of cost and fuel economy as the energy storage system in a fuel cell based hybrid electric vehicle," *J. Power Sources*, vol. 196, no. 3, pp. 1163–1170, 2011.
- [31] M. Masih-Tehrani, M.-R. Ha'iri-Yazdi, V. Esfahanian, and A. Safaei, "Optimum sizing and optimum energy management of a hybrid energy storage system for lithium battery life improvement," *J. Power Sources*, vol. 244, pp. 2–10, 2013.



He Yin (S'13) received the B.S. degree in electrical and computer engineering from University of Michigan-Shanghai Jiao Tong University Joint Institute, Shanghai Jiao Tong University, Shanghai, China in 2012. He is currently working toward Ph.D. degree in the same institute.

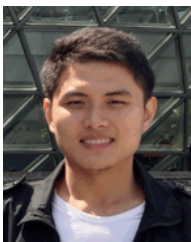
His research interests include optimization and decentralized control of hybrid energy storage systems and wireless power transfer systems.



Chengbin Ma (M'05) received the B.S. (Hons.) degree in industrial automation from East China University of Science and Technology, Shanghai, China, in 1997, and the M.S. and Ph.D. degrees both in electrical engineering from University of Tokyo, Japan, in 2001 and 2004, respectively.

He is currently an assistant professor of electrical and computer engineering with the University of Michigan-Shanghai Jiao Tong University Joint Institute, Shanghai Jiao Tong University, China. He is also with a joint faculty appointment in School of Mechanical Engineering, Shanghai Jiao Tong University. Between 2006 and 2008, he held a post-doctoral position with the Department of Mechanical and Aeronautical Engineering, University of California Davis, USA. From 2004 to 2006, he was a R&D researcher with Servo Laboratory, Fanuc Limited, Japan.

His research interests include networked hybrid energy systems, wireless power transfer, and mechatronic control.



Chen Zhao (S'14) received the B.S. degree in electrical engineering automation from the East China University of Science and Technology, Shanghai, China, in 2011. He is currently working toward the Ph.D. degree in electrical and computer engineering at the University of Michigan-Shanghai Jiao Tong University Joint Institute, Shanghai Jiao Tong University, Shanghai.

His research interests include modeling and testing of lithium-ion batteries and control of battery-ultracapacitor hybrid energy storage systems.